

SYNTHESIS AND CHARACTERIZATION OF CITRIC ACID ASSISTED Cr DOPED LITHIUM MANGANESE OXIDE SPINEL

GURPREET SINGH, AMRISH PANWAR*, ANJAN SIL, SUDIPTO GHOSH*

*Department of Metallurgical and Materials Engineering,
Indian Institute of Technology Roorkee, Roorkee 247 667, Uttarakhand, India*

**Department of Metallurgical and Materials Engineering,
Indian Institute of Technology Kharagpur, Kharagpur 721 302, West Bengal, India*

E-mail: anj_sil@yahoo.co.uk

Submitted January 13, 2009; accepted August 7, 2009

Keywords: Sol-gel, Spinel structure, X-ray diffraction, Differential scanning calorimetry, Discharge capacity

The powders in the system $\text{LiCr}_x\text{Mn}_{2-x}\text{O}_4$ ($0.0 \leq x \leq 0.5$) were synthesized by sol-gel method using citric acid as a chelating agent. The powders were characterized by X-ray diffraction (XRD), Field emission scanning electron microscopy (FESEM), Differential scanning calorimetry (DSC), Impedance spectroscopy (IS) and Electrochemical analysis. Change in particle morphology from truncated octahedral (tetradecahedra) to perfect octahedron for the higher doping concentration of Cr has been reported. Decrease in particle size has been observed with the increase in Cr content. The stability in the crystalline structure of LiMn_2O_4 cubic spinel over the temperature range of battery operation was achieved by chromium doping. The electrical conductivity at room temperature of the powdered samples in various compositions studied is of $\sim 10^{-5}$ S/cm. Electrochemical analyses of the materials in all the compositions were carried out in the voltage range of 4.3 V to 3.0 V. The cubic to cubic phase transition in LiMn_2O_4 which occurs at around 4.15 V can be suppressed by Cr doping. The discharge capacity of the compound is maximum of ~ 130 mAh/g for the composition $x = 0.0$. The capacity decreases with increase in doping concentration and becomes minimum of ~ 80 mAh/g at $x = 0.5$.

INTRODUCTION

LiCoO_2 is a well known cathode material for rechargeable lithium ion batteries [1]. However, due to its high cost and toxicity, there has been a continuous demand for the last few years to develop alternative cathode materials which will be environment friendly and cost effective. Manganese based LiMn_2O_4 [2], LiMnO_2 [3] and olivine type LiFePO_4 [4] are promising materials for future to substitute LiCoO_2 . These alternative materials are non-toxic and cheaper [5] as compared to LiCoO_2 . However, the manganese based cathode materials have also drawbacks. The discharge capacity of the manganese based materials is low and is about 80% that of LiCoO_2 . LiFePO_4 has lower electrical conductivity than that of LiCoO_2 , which however, can be improved significantly either by carbon coating [6] or by doping with one or more of the following elements Mg, Al, Ti and Nb [7]. The electrochemical study of LiMn_2O_4 has established that structural distortion of the cubic spinel phase occurs after a few cycles of charging and discharging. Such distortion leads to structural transformation in the spinel from cubic to tetragonal. In LiMn_2O_4 cubic spinel, Mn exists in 3+ and 4+ valence states. The Mn^{3+} ions cause the structural change in LiMn_2O_4 leading to capacity fading [2, 8, 9] during recycling. The distortion caused by Mn^{3+} in the cubic structure is known as Jahn-Teller (J-T) distortion. A significant effort has been made by the

researchers to reduce the J-T distortion in LiMn_2O_4 and LiMnO_2 by doping with one of more elements of Mg, Cr, V, Ti, Al, Fe, Zn [10-15] which are divalent or trivalent. A detailed cyclic voltammetry study on $\text{LiCr}_x\text{Mn}_{2-x}\text{O}_4$ revealed that chromium substitution upto $x \leq 0.62$ is useful for attaining desired characteristics including retaining structural stability of the cubic spinel phase [16]. Such substitution also stabilizes the cubic spinel structure.

Sol-gel route is a promising method for preparation of LiMn_2O_4 and LiMnO_2 cathode materials. Uniform particle size in the sub-micron range could be obtained by the sol-gel method. R. Thirunakaran et al. used adipic acid as well as oxalic acid as chelating agents in sol-gel synthesis of chromium doped LiMn_2O_4 . The pH of the solution in their study was maintained between 7.0 and 8.5 and the powder was calcined at 800°C [17, 18]. Particles having spherical morphology and of uniform size in the sub-micron range were obtained in their studies.

It was also found that LiMn_2O_4 in nanocrystalline size prepared by ball milling shows much better cyclability than that has larger particle size [19]. In the present investigation, an attempt was made to synthesize the single phase nanocrystalline $\text{LiCr}_x\text{Mn}_{2-x}\text{O}_4$ cubic spinel following chemical synthesis technique viz. sol-gel process. Citric acid was used as a chelating agent. The chromium concentration, the pH value of the precursor

solution and the calcination temperature were suitably adjusted so as to develop $\text{LiCr}_x\text{Mn}_{2-x}\text{O}_4$ as nanocrystalline materials having cubic spinel structure with prismatic morphology. The powders obtained were characterized by X-ray diffraction analysis, Field emission scanning electron microscopy, Differential scanning calorimetry, Impedance spectroscopy, Electrochemical analysis techniques.

EXPERIMENTAL

Lithium acetate $\text{Li}(\text{CH}_3\text{COO})\cdot\text{H}_2\text{O}$ (LOBA CHEMIE, 99%), manganese acetate $\text{Mn}(\text{CH}_3\text{COO})_2\cdot 4\text{H}_2\text{O}$ (MERCK, $\geq 99.5\%$) and chromium nitrate $\text{Cr}(\text{NO}_3)_3\cdot 9\text{H}_2\text{O}$ (LOBA CHEMIE, 98%) were used as raw materials. Saturated solutions of these materials were prepared separately and these solutions were mixed. The *pH* of the mixed solution was maintained at around 7.0 using ammonium hydroxide solution. Citric acid was added to the solution, with a molar ratio of 1:1 maintained between the citric acid and the total metal ions required to form $\text{LiCr}_x\text{Mn}_{2-x}\text{O}_4$ compounds. The solution mixture was heated in the temperature range of 80-90°C with a continuous stirring until a thick gel was obtained. The resulting gel was heated to 350°C for 2 hours to decompose the acetates and nitrates. The powder thus obtained was calcined at 750°C for 12 hours.

X-ray diffraction (XRD) patterns of the powdered samples were obtained by X-ray diffractometer (D8 Advance Bruker AXS embedded with fast detector) using $\text{CuK}\alpha$ radiation having wavelength of 1.54 Å. Step size and dwell time for each step in the X-ray scan were 0.0198° and 0.5 seconds respectively. Phase analysis was carried out from the XRD patterns obtained and the lattice parameters were determined using Rietveld refinement by using X'Pert high score plus software. The guidelines for the Rietveld refinement mentioned by L. B. McCusker et. al. [20] has been taken in to account.

Microstructural investigation of the calcined powders was carried out using Field emission scanning electron microscope (FESEM) (Supra 40 Carl ZEISS). Thermal analyses were carried out by Differential scanning calorimeter (DSC) (Perkin Elmer) in presence of argon gas. The temperature range for the DSC measurements was -40°C to +60°C with a heating rate of 5°C/min.

Impedance measurements at room temperature of the samples prepared from calcined powders were made by using impedance analyzer (Agilent 4294A) in the frequency range of 40 Hz to 10 MHz. All the measurements were done at an oscillation level of 10 mV. Each sample was made in the form of cylindrical pellet having 10 mm diameter by taking 300 mg of calcined powder and compacting them with a suitable load. The flat surfaces of these pellets were applied with silver paste followed by baking at ~140°C for electroding.

Electrochemical studies on the materials were performed in a laboratory made cell testing set-up consisting of teflon and stainless steel screw as shown in Figure 1. Experiments were performed in the argon filled glove box (MBRAUN) in which the water and oxygen level was maintained below 0.1 ppm. At first the powders were mixed with acetylene black and PVDF in the ratio of 70:15:15 (wt.%) respectively. A slurry of the powder mixture was made using N-Methylpyrrolidone (NMP) and applied by using a blade onto aluminum foil for coating. The coating was dried in vacuum oven at 120°C for 24 hours. Electrodes of about ~1 cm² area were cutout from the foil. A thin strip of lithium metal was used as reference electrode. Celgard (2400) was used as a separator. 1M LiPF_6 dispersed in EC and DEC in 1:1 v/v was used as electrolyte. Electrical contacts were drawn using stainless steel screws. Cells were charged and discharged at a constant current density of 100 $\mu\text{A}/\text{cm}^2$ in a voltage range of 4.3 V to 3.0 V.

RESULTS AND DISCUSSION

The synthesized $\text{LiCr}_x\text{Mn}_{2-x}\text{O}_4$ powders were characterized using XRD for determination of crystal structure. The XRD patterns of $\text{LiCr}_x\text{Mn}_{2-x}\text{O}_4$ are shown in Figure 2a. Analysis of the XRD patterns shows the formation of single phase cubic spinel for all the compositions with a space group of $\text{Fd}\bar{3}\text{m}$. Lattice parameters of the compounds synthesized with different doping levels of Cr were determined by Rietveld refinement. Stripping of the $\text{CuK}\alpha_2$ and background determination has not been performed. The results of the refinement analysis of various compounds are shown in Figure 2b. The XRD analyzed data for all the compositions are given in Table 1. The lattice parameters thus obtained were plotted as a function of Cr concentration in Figure 3. It can be noticed from the Figure 3 that with the increase in the chromium concentration, a gradual decrease in lattice parameter leading to lattice contraction takes place.

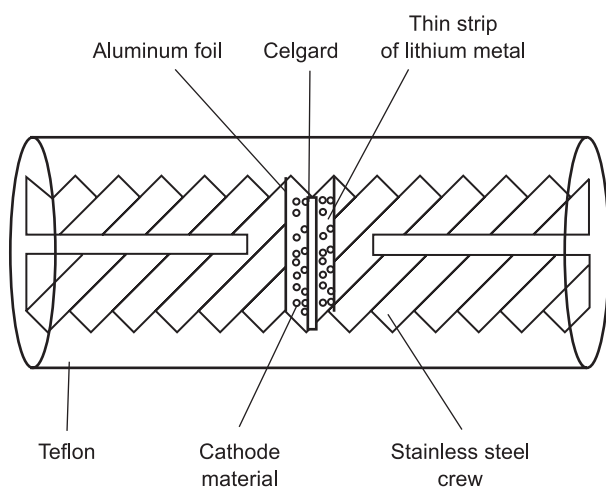


Figure 1. Schematic diagram of Teflon-stainless steel screw raw cell testing arrangement for electrochemical performance.

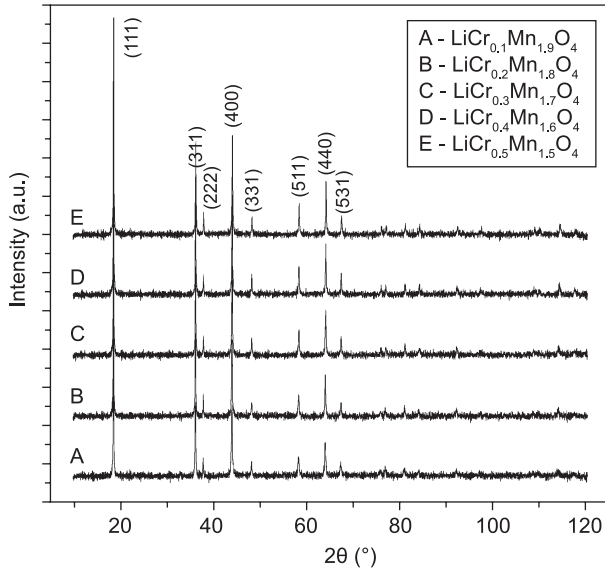


Figure 2a XRD patterns of $\text{LiCr}_x\text{Mn}_{2-x}\text{O}_4$; $x = 0.0, 0.1, 0.2, 0.3, 0.4$ and 0.5 .

This is due to the replacement of larger Mn^{3+} (0.68 \AA) ions by smaller Cr^{3+} (0.615 \AA) ions [17]. A clear shift in the peak position (Figure 4) towards higher angles can be seen by expanding the scale of the XRD patterns in the 2θ range of $18\text{--}19^\circ$. This indicates the decrease in lattice constant with the increase in Cr content. It has been shown that the capacity of cell decreases as the Cr concentration is increased. However, the decrease in capacity is acceptable only up to $x = 0.5$ in $\text{LiCr}_x\text{Mn}_{2-x}\text{O}_4$ [12].

DSC analysis on LiMn_2O_4 , as shown in Figure 5, shows phase transformation at a temperature of $\sim 286 \text{ K}$ (13°C). It was demonstrated by the researchers that the phase transition is closely related to the presence of oxygen vacancies in the structure and hence non-stoichiometry of the compound. Existence of oxygen vacancy is essential for the phase transition [21]. Compound having perfect stoichiometry does not show any kind of phase transition over the temperature region

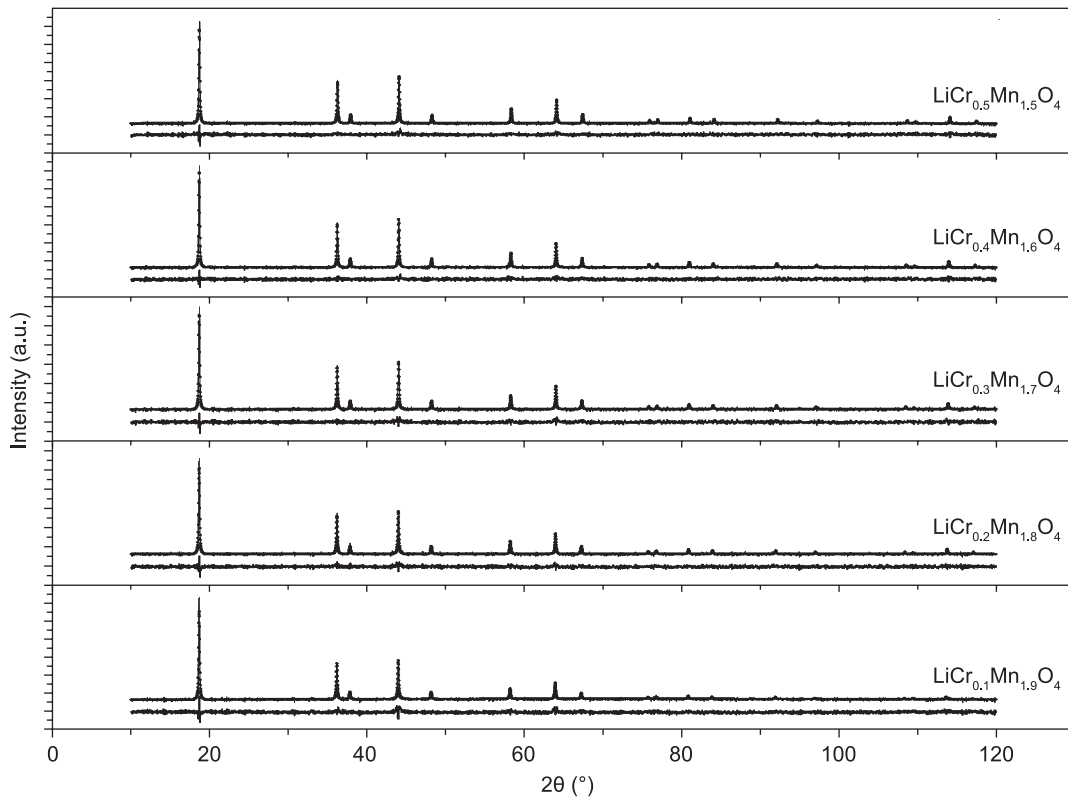


Figure 2b Refinement analysis patterns for various compositions. — I_{cal} ; • I_{obs} ; The lower profile is the difference $I_{\text{obs}} - I_{\text{cal}}$

Table 1. XRD data of LiMn_2O_4 and doped with Cr after Rietveld refinement.

	X = 0	X = 0.1	X = 0.2	X = 0.3	X = 0.4	X = 0.5
Lattice parameter (\AA)	8.237(2)	8.228(2)	8.223(2)	8.217(1)	8.213(2)	8.206(1)
Cell volume (\AA^3)	558.86	557.18	556.15	554.79	554.10	552.66
R_{wp} (%)	6.54	7.40	6.98	6.93	6.99	7.38
R_{p} (%)	5.45	5.81	5.51	5.50	5.58	5.84
GOF	1.20	1.64	1.37	1.41	1.48	1.50
Density (g/cm^3)	4.297	4.303	4.304	4.307	4.306	4.310

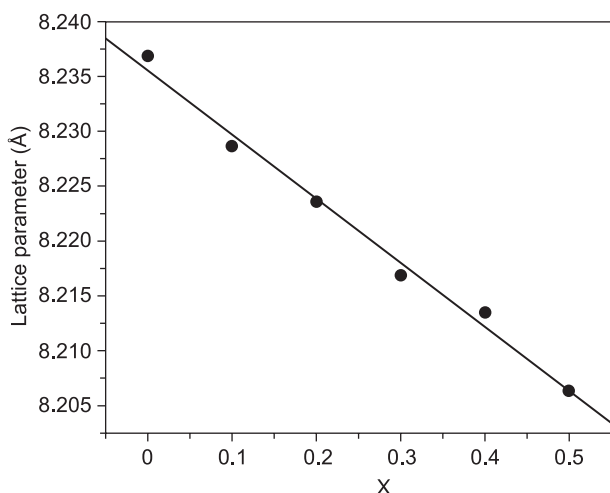


Figure 3. Variation of lattice parameter of $\text{LiCr}_x\text{Mn}_{2-x}\text{O}_4$ with x between $x = 0.0-0.5$.

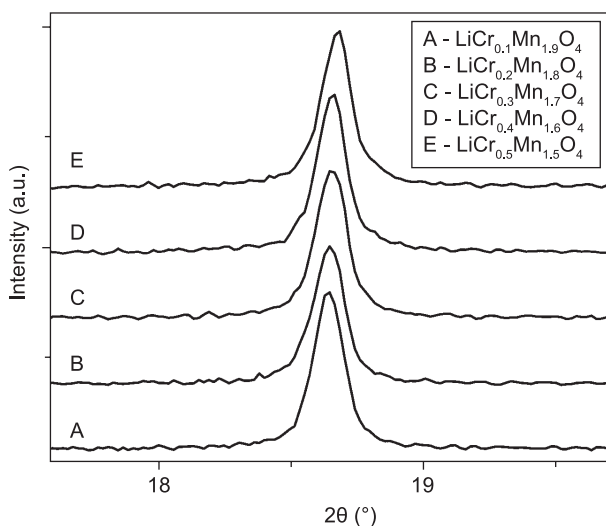


Figure 4. Shifting of the peak position in the system $\text{LiCr}_x\text{Mn}_{2-x}\text{O}_4$ ($0.0 \leq x \leq 0.5$).

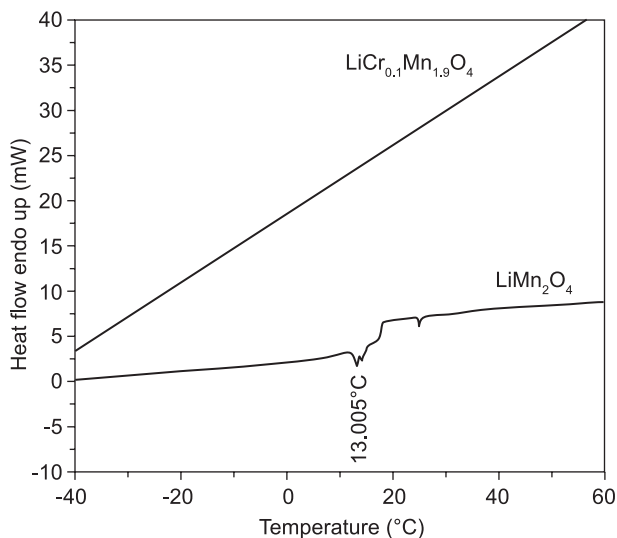


Figure 5. DSC traces of LiMn_2O_4 and $\text{LiCr}_{0.1}\text{Mn}_{1.9}\text{O}_4$ compounds.

stated above. It can be seen in the Figure 5 that the compound with composition $x = 0.1$ does not undergo phase transformation in the working temperature range of battery, signifying that the Cr doping results in structural stability in LiMn_2O_4 . Similarly the doping with higher Cr concentration ($x = 0.2-0.5$), structural transformation does not occur. Therefore, the structural transformation which occurs in LiMn_2O_4 , can be avoided by Cr doping. FESEM micrographs of $\text{LiCr}_x\text{Mn}_{2-x}\text{O}_4$ ($0.0 \leq x \leq 0.5$) powders, as shown in Figure 6, show that the powders are of nano size. The particle size varies from ~ 50 nm to ~ 150 nm. The facet like appearance is more with higher Cr doping level i.e. for $x = 0.4$ and 0.5 . A clear change in particle morphology from truncated octahedral (tetradecahedra) to perfect octahedron can be seen from the FESEM micrographs. To the best of authors' knowledge such a change in the particle morphology with the increase in Cr concentration has been reported for the first time in the literature. Such a change in morphology can be explained on the basis of change in the kinetics of grain growth with the increase in Cr content. Such well defined faceted structures are important in understanding intradomain interaction and grain fracture as a result of cycling [22]. On the whole, the particle size decreases, with increase in x for the system $\text{LiCr}_x\text{Mn}_{2-x}\text{O}_4$ studied. This is in agreement with the observations on the same system $\text{LiCr}_x\text{Mn}_{2-x}\text{O}_4$ obtained through solid state routes [23]. S.Shi et.al. [24] used local density approximation (LDA) and pseudopotential plane wave method as implemented in Vienna ab-initio simulation package (VASP) for pure LiMn_2O_4 and $\text{LiCr}_x\text{Mn}_{2-x}\text{O}_4$ structures. It was shown by them that Cr doped structures are energetically more stable as compared to that of undoped LiMn_2O_4 . The decrease in particle size is perhaps due to increase in the stability of $\text{LiCr}_x\text{Mn}_{2-x}\text{O}_4$ with x , as shown by ab-initio study [24]. As Gibbs free energy change ΔG increases, the drive for nucleation of particle increases and the rate of nucleation perhaps increases as compared to that of the growth, resulting in lower particle size.

The use of adipic acid and oxalic acid as chelating agent yields particles having spherical morphology with an average size in the nano range ~ 100 nm to ~ 200 nm [17,18]. The agglomeration in particles develops with the increase in chromium content. Such kind of agglomeration was found to be beneficial because this feature offers good packing density and inter-particle contact [18]. This trend was similar to that observed by Thirunakaran et. al. with other chelating agents. Thus the Cr substitution was supportive in providing a better morphology of the powder from the point of view of electrochemical performance.

Impedance measurements for various frequencies were made on the samples having a shape of cylindrical pellet. Real and imaginary parts of the measured impedance values were plotted in a complex plane and are shown in Figure 7. Bulk resistances of the samples were

calculated from the extrapolated semicircular plots on the resistance axis. The electrical conductivities (σ) for all the samples were calculated using the following relation

$$\sigma = (1/R) \times (l/A)$$

where l is thickness and A the area of the cylindrical samples [25]. The conductivity values for various compositions are given in Table 2. Figure 8 shows the variation of real part of impedance (Z') with frequency. A regular increase in the impedance value at low frequen-

cy was found with the increase in Cr content. While it can be seen from the Figure 8 that the impedance values for all the compositions are same at higher frequencies ($\sim 1 \times 10^{-3} \text{ M}\Omega$ at 10^7 Hz). This shows that polarization was small at low frequencies for lightly doped spinel and the polarization increases with the increase in chromium concentration. Figure 9 shows the loss spectrum (i.e. the variation of imaginary part of impedance (Z'') with frequency). Peaks with higher intensity were obtained at higher Cr content compared to

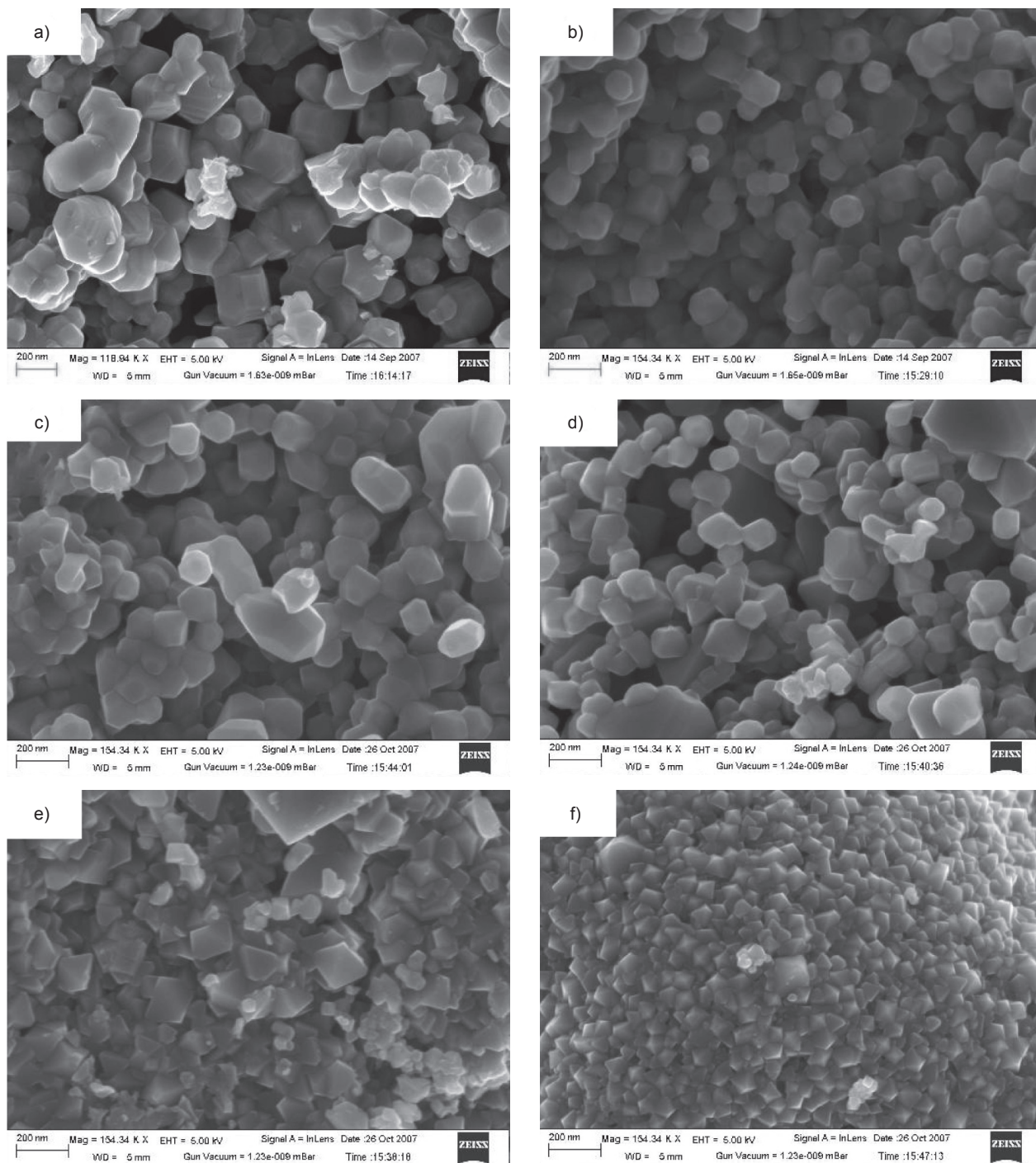


Figure 6. FESEM micrographs of calcined powders in the system $\text{LiCr}_x\text{Mn}_{2-x}\text{O}_4$: a) $x = 0.0$; b) $x = 0.1$; c) $x = 0.2$; d) $x = 0.3$; e) $x = 0.4$; f) $x = 0.5$.

that of the compositions having low chromium content. Peak width (related to relaxation time) [26] was found to decrease with the increase in chromium content. Since relaxation is generally caused by the delay in molecular polarization with respect to changing electric field, therefore relaxation process in this case was found to be composition dependent phenomenon. Further the magnitude of Z'' increases with the increase in chromium content and the value of the frequency at which this maxima occurs shift towards the lower frequency. Such kind of spectrum probably arises due to the presence of space charge in the material [26].

Table 2. Electrical Conductivity values for various compositions.

Composition	Electrical conductivity value (S/cm)
$\text{LiCr}_{0.1}\text{Mn}_{1.9}\text{O}_4$	6.61×10^{-5}
$\text{LiCr}_{0.2}\text{Mn}_{1.8}\text{O}_4$	3.93×10^{-5}
$\text{LiCr}_{0.3}\text{Mn}_{1.7}\text{O}_4$	3.67×10^{-5}
$\text{LiCr}_{0.4}\text{Mn}_{1.6}\text{O}_4$	2.53×10^{-5}
$\text{LiCr}_{0.5}\text{Mn}_{1.5}\text{O}_4$	1.57×10^{-5}

Charge and discharge curves for various samples were obtained within a voltage range of 4.3 to 3.0 V. Curves for the various compositions are shown in Figure 10. It was found that discharge profile becomes flatter with the increase in Cr concentration, with the voltage step at 4.15 V that exists for LiMn_2O_4 , becomes vanishingly small with the increase in Cr concentration. This perhaps indicates the suppression of cubic to cubic structural transition. The discharge capacity was found to decrease with the increase in chromium concentration. However, the fall in capacity after 10 cycles of charging and discharging is less in the case of Cr doped compounds as compared to that of pure LiMn_2O_4 . The capacity fall also decreases with the increase in Cr concentration. Figure 11 shows plot of discharge capacity as a function of cycle number (shown upto first 10 cycles) for the samples doped with Cr of various concentrations. The fall in capacity with the increase in Cr concentration can be explained on the basis of the fact that with the increase in Cr content, the concentration of Mn^{3+} ions decreases and the concentration of Mn^{4+} ions increases. The ideal composition in which Mn^{3+} is totally absent is $\text{Li}_4\text{Mn}_5\text{O}_{12}$. Unfortunately, such compound practically possesses no capacity in 4V region because the oxidation of Mn^{4+} cations was not possible by lithium extraction.

In the case of pure LiMn_2O_4 a tail at the end of discharge (capacity at around 3.2 V) can be seen. But for the Cr doped samples no such tail was observed. It can be correlated in terms of oxygen deficiency in the samples of pure LiMn_2O_4 as reported earlier [27]. This was also in agreement with our DSC measurements. Since the peak in DSC curve is highly sensitive to the oxygen non stoichiometry, hence if the composition is oxygen deficient it will show some capacity at around 3.2 V.

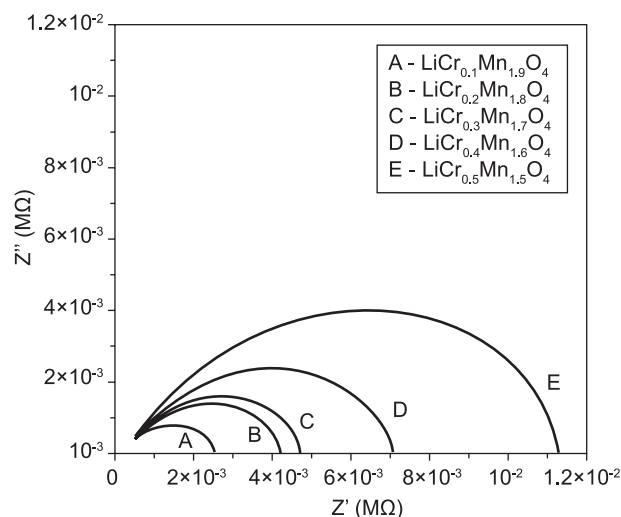


Figure 7. Complex impedance spectra (Nyquist plots) of powdered samples in the system $\text{LiCr}_x\text{Mn}_{2-x}\text{O}_4$ ($0.0 \leq x \leq 0.5$).

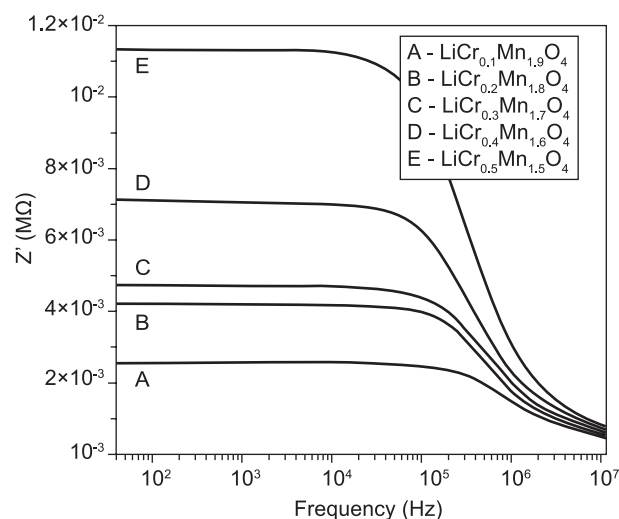


Figure 8. Variation of real part of impedance (Z') with frequency of measurements.

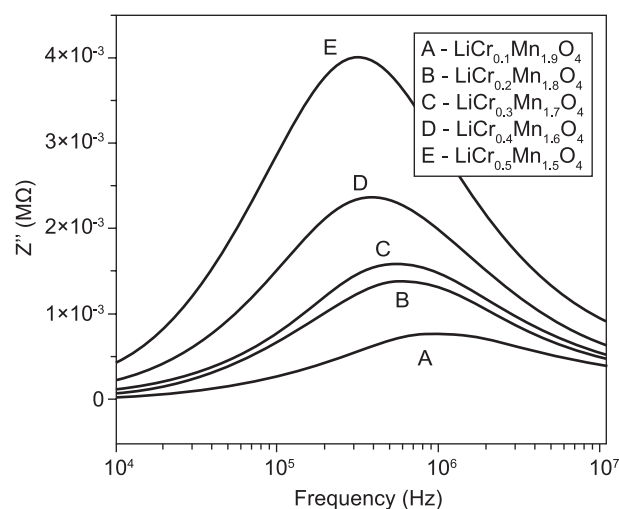


Figure 9. Variation of imaginary part of impedance (Z'') with frequency of measurements.

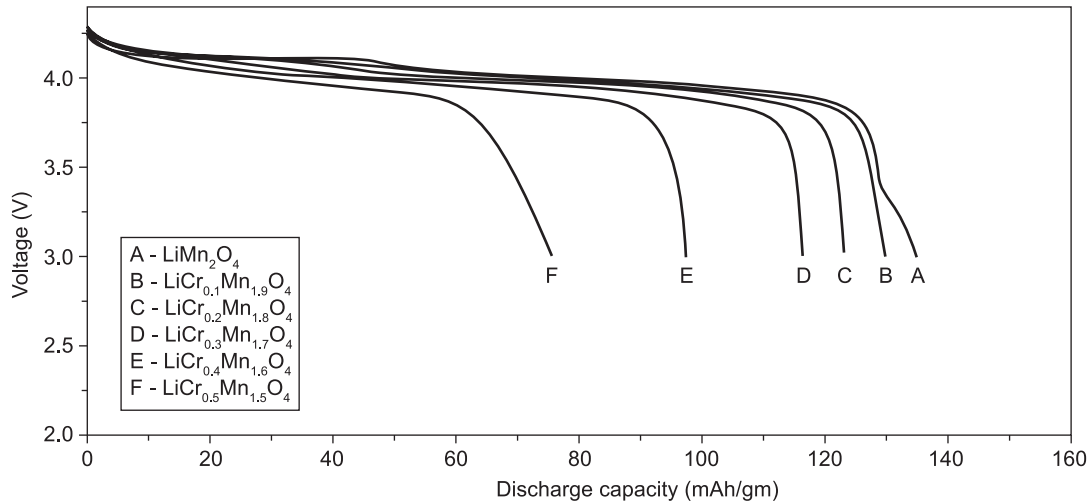


Figure 10. Discharge capacity profiles of $\text{LiCr}_x\text{Mn}_{2-x}\text{O}_4$ ($0.0 \leq x \leq 0.5$) on first cycle.

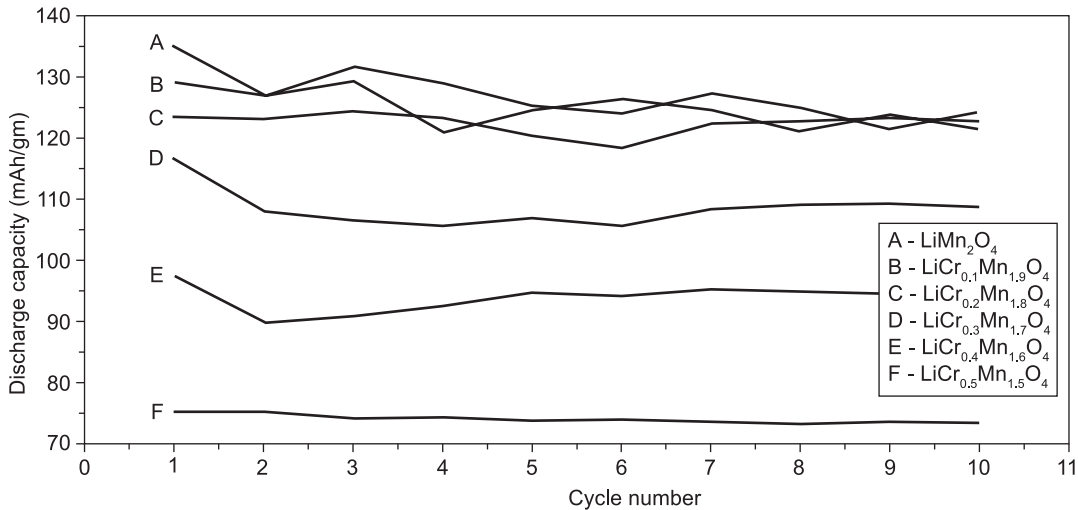


Figure 11. XRD pattern of the sample modified by the addition 50 wt.% of silane.

CONCLUSIONS

1. Citric acid assisted sol-gel synthesis is found to be promising technique for the chromium doping in LiMn_2O_4 .
2. Desirable morphological and agglomeration characteristics of the synthesized powders have been achieved by this method.
3. Stability of LiMn_2O_4 over a temperature range of battery operation can be obtained by doping with even 10 mol.% of chromium.
4. Electrical conductivity values for the various compositions are found to be of the order of $\sim 10^{-5}$ S/cm.
5. Chromium acts as a promising dopant for the suppression of cubic-cubic transition at around 4.15 V in the discharge profile of LiMn_2O_4 .
6. Discharge capacity of ~ 130 mAh/g has been achieved in undoped LiMn_2O_4 and the capacity decreases with the increase in chromium concentration. The discharge capacity becomes ~ 80 mAh/g for the dopant concentration of $x = 0.5$.

References

1. Mizushima K., Jones P. C., Wiseman P. J., Goodenough J. B.: Mater. Res. Bull. 15, 783 (1980).
2. Thackeray M. M., David W. I. F., Bruce P. G., Goodenough J. B.: Mater. Res. Bull. 18, 461 (1983).
3. Davidson I. J., McMillan R. S., Murray J. J., Greedan J. E.: J. Power Sources. 54, 232 (1995).
4. Padhi A.K., Nanjundaswamy K.S., Goodenough J.B.: J. Electrochem. Soc. 144, 1188 (1997).

5. Feng Li, Chang Yuqin, Wu Lie, Tianhong Lu: *J. Power Sources*. *63*, 149 (1996).
6. Cao Q., Zhang H.P., Wang G.J., Xia Q., Wu Y.P., Wu H.Q.: *Electrochem. Comm.* *9*, 1228 (2007).
7. Chung Sung-Yoon, Bloking Jason T., Chiang Yet-Ming: *Nature Mater.* *1*, 123 (2002).
8. Thackeray M. M., De Picciotto L.A., De Kock A., Johnson P. J., Nicholas V., Adendorff K.: *J. Power Sources* *21*, 1 (1987).
9. Yamada A., Tanaka M.: *Mater. Res. Bull.* *30*, 715 (1995).
10. Jeong In-Seong, Kim Jong-Uk, Gu Hal-Bon: *J. Power Sources*. *102*, 55 (2001).
11. Capsoni D., Bini M., Chiodelli G., Massarotti V., Mozzati M. C., Azzoni C. B.: *Solid State Comm.* *125*, 179 (2003).
12. Sigala C., Le Gal La Salle A., Piffard Y., and Guyomard D.: *J. Electrochem. Soc.* *148*, A826 (2001).
13. Song D., Ikuta H., Uchida T., Wakihara M.: *Solid State Ionics* *117*, 151 (1999).
14. Kumar Gopu., Schlorb H., Rahner D.: *Mater. Chem. Phys.* *70*, 117 (2001).
15. Feng Qi., Hanoh H., Miyai Y., Ooi K.: *Chem. Mater.* *7*, 379 (1995).
16. Sigala C., Le Gal La Salle A., Piffard Y., Guyomard D.: *J. Electrochem. Soc.* *148*, A826 (2001).
17. Thirunakaran R., Kim Ki-Tae, Kang Yong-Mook, Seo Chan-Yeo, Jai Young-Lee: *J. Power Sources* *137*, 100 (2004).
18. Thirunakarana R., Kim Ki-Tae, Kang Yong-Mook, Jai Young-Lee: *Mater. Res. Bull.* *40*, 177 (2005).
19. Kang Sun-Ho, Goodenough John B., Rabenberg Llewellyn K.: *Electrochem. and Solid State Lett.* *4*, A49 (2001).
20. McCusker L. B., Von Dreele R. B., Cox D. E., Loue Er D., Scardi P.: *J. Appl. Cryst.* *32*, 36 (1999).
21. Yang X.Q., Sun X., Balasubramanian M., McBreen J., Xia Y., Sakai T., Yoshio M.: *Electrochem. and Solid State Lett.* *4*, A117 (2001).
22. Wen W., Kumarasamy B., Mukerjee S., Auinat M., Ein-Elilb Y.: *J. Electrochem. Soc.* *152*, A1902 (2005).
23. Wang H.-C., Lu C.-H.: *J. Power Sources* *119*, 738 (2003).
24. Shi S., Wang D.-S., Meng S., Chen L., Huang X.: *Phys. Rev. B* *67*, 115130 (2003).
25. Maia Luciana F., Rodrigues Ana C. M.: *Solid State Ionics* *168*, 87 (2004).
26. Chatterjee Sandeep, Mahapatral P. K., Choudhary R. N. P., Thakur Awalendra K.: *Phys. Stat. Sol.* *201*, 588 (2004).
27. Gao Y., Dahn J. R.: *J. Electrochem. Soc.* *143*, 100 (1996).